Bull. Mater. Sci., Vol. 37, No. 6, October 2014, pp. 1535–1542. © Indian Academy of Sciences.

One-step electrodeposition process of $CuInSe_2$: Deposition time effect

O MEGLALI[a,*], N ATTAF[a], A BOURAIOU[b], M S AIDA[a] and S LAKEHAL[c]

[a]Thin Films and Interfaces Laboratory, Department of Physics, Mentouri University, Constantine 25000, Algeria
[b]Sciences and Technologies Faculty, Ziane Achour University, Djelfa 17000, Algeria
[c]Ceramics Laboratory, Mentouri University, Constantine 25000, Algeria

MS received 14 March 2013; revised 4 August 2013

Abstract. **$CuInSe_2$ thin films were prepared by one-step electrodeposition process using a simplified two-electrodes system. The films were deposited, during 5, 10, 15 and 20 min, from the deionized water solution consisting of $CuCl_2$, $InCl_3$ and SeO_2 onto ITO-coated glass substrates. As-deposited films have been annealed under vacuum at 300 °C during 30 min. The structural, optical band gap and electrical resistivity of elaborated films were studied, respectively, using X-ray diffraction (XRD), Raman spectroscopy, UV spectrophotometer and four-point probe method. The micro structural parameters like lattice constants, crystallite size, dislocation density and strain have been evaluated. The XRD investigation proved that the film deposited at 20 min present $CuInSe_2$ single phase in its chalcopyrite structure and with preferred orientation along (1 1 2) direction, whereas the films deposited at 5, 10 and 15 min show the $CuInSe_2$ chalcopyrite structure with the In_2Se_3 as secondary phase. We have found that the formation mechanism of $CuInSe_2$ depends on the In_2Se_3 phase. The optical band gap of the films is found to decrease from 1·17 to 1·04 eV with increase in deposition time. All films show Raman spectra with a dominant A_1 mode at 174 cm^{-1}, confirming the chalcopyrite crystalline quality of these films. The films exhibited a range of resistivity varying from 2.3×10^{-3} to 4.4×10^{-1} Ω cm.**

Keywords. **Electrodeposition; $CuInSe_2$; deposition time; thin films.**

1. Introduction

Chalcopyrite, $CuInSe_2$, is considered one of the most important semiconductors that can be used to make low-cost photovoltaic devices. It has high absorption coefficient ($> 10^5$ cm^{-1}) (Kavcar *et al* 1992; Huang *et al* 2004), reasonable work function and suitable band gap, and this semiconductor can be used for the preparation of the homojunctions or heterojunctions (Rincon *et al* 1983). Efficiency of 19·9% for laboratory-scale solar cell and of 13% for commercial modules have been achieved by using $CuInSe_2$ thin films as absorber layers (Wellings *et al* 2009); these progresses open new perspectives.

Various techniques such as close-spaced vapour transport (CSVT) (Zouaoui *et al* 1999), RF sputtering (Parretta *et al* 1993), co-evaporation (Moharram *et al* 2001), spray (Tembhurkar and Hirde 1994), molecular beam epitaxy (White *et al* 1979), electrodeposition (Fahoume *et al* 1998), chemical bath deposition (Murali 1988), etc. have been adopted for the growth of $CuInSe_2$ films. Amongst them, electrodeposition is an appealing technique that offers low cost of equipment, no use of toxic gases, high rate deposition and scalability for large-area thin films deposition. This technique can be used as a one-step process (co-deposition) or a multi-step process. The one-step electrodeposition is the common method adopted for laboratory-scale devices, Moorthy Babu *et al* (2005) found that the $CuInSe_2$ films electrodeposited with one-step electrodeposition have better adherence, low porosity and are stable during characterization processes. The electrodeposition technique has already been proven for $CuInSe_2$ solar cells with a record efficiency of 10% for laboratory-scale devices and 6–7% for 30×30 cm^2 modules (Wellings *et al* 2009).

In this work, we have grown $CuInSe_2$ by one-step electrodeposition technique. Films were deposited at various deposition times onto indium thin oxide (ITO)-covered glass substrates. We also investigated the influence of deposition time on the structure, microstructure and optical properties of electrodeposited films.

2. Experimental

$CuInSe_2$ thin films were deposited using a sample two-electrode cell configurations. The counter electrode was a platinum sheet and the ITO layer-coated glass substrates ($15 \times 5 \times 1{\cdot}1$ mm) were used as the working electrodes.

Before deposition of the films, the ITO-coated glass cathode was first washed with distilled water, ultrasonically cleaned with acetone and, finally, washed with distilled water jets and dried. After each film deposition, the

*Author for correspondence (meglali2@yahoo.fr)

platinum anode was polished with fine emery paper, washed with distilled water and ultrasonically cleaned with acetone.

The electrolytic solution prepared using 10 mM $CuCl_2$, 20 mM $InCl_3$ and 20 mM SeO_2 (1 : 2 : 2 ratio) dissolved in deionized water. The pH of the solution was around 2·6 and the solution was prepared just prior to the commencement of the elaboration.

The $CuInSe_2$ thin films were deposited at the following deposition times: 5, 10, 15 and 20 min. The applied potential was fixed at –7 V and the deposition was carried out at room temperature without stirring the solution. After completion of the deposition, the films were rinsed in deionized water and dried in air. The as-deposited films were annealed under vacuum at 300 °C during 30 min.

The structural and optical aspects of the films were analysed. The crystalline structure was studied by means of X-ray diffraction (XRD) using CuKα1 radiation of wavelength λ = 1·54056 Å, scans were performed in the range of 15–90°. The operation voltage and current used are, respectively, 30 kV and 40 mA. The optical transmittance as a function of the incident wavelength was recorded, at room temperature, in the wavelength range from 200 to 1800 nm using UV–Vis–NIR spectrophotometer (Shimadzu UV-3101 model). An identical ITO coated glass substrate was used as reference for recording the optical absorption spectra. The films thickness, *d*, was estimated theoretically using the following formula (Faraday 1834)

$$d = \frac{1}{nFA}\left(\frac{itM}{\rho}\right). \quad (1)$$

Here *n* is the number of electrons transferred, *F* Faraday's number, *A* the electrode area, *i* the applied current, *t* the deposition time, *M* and ρ are, respectively, the molecular weight and the density of $CuInSe_2$ material.

For our calculations, we used the formula weight (336·28 g mol^{-1}) and density (5·77 g cm^{-3}) of intrinsic CIS. The number of electrons transferred was taken as 13 according to the total electrode reaction (Weast 1980)

$$Cu^{2+} + In^{3+} + 2SeO_3^{2-} + 12H^+ + 13e^- \rightarrow CuInSe_2 + 6H_2O. \quad (2)$$

Raman spectra of the films in the range of 50–450 cm^{-1} were performed at room temperature using micro Raman system (SENTERRA Raman microscope) with spectral resolution of 0·5 cm^{-1} and with 532 nm wavelength as light source. The electrical resistivity of the films was carried out by four-point probe method.

3. Results and discussion

The films thickness evolution vs deposition time is shown in figure 1. It is easily seen that the films thickness increases quasi-linearly with deposition time, and it ranged between 0·3 and 0·9 μm.

Figure 2(a–d) shows the XRD patterns of the annealing films as a function of deposition time ((a): 5, (b): 10, (c):

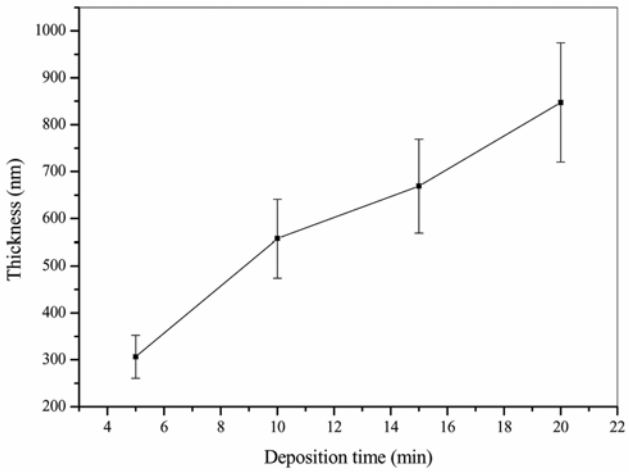

Figure 1. Variation of film thickness vs deposition time.

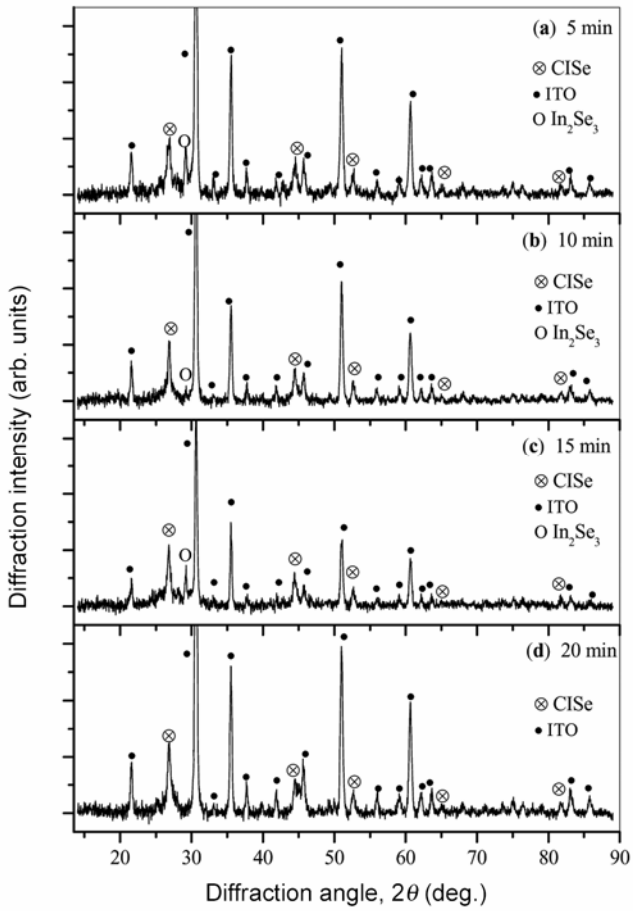

Figure 2. XRD patterns of $CuInSe_2$ deposited on ITO-coated glass substrate after annealing under vacuum at 300 °C during 30 min related to different deposition times: (**a**) 5, (**b**) 10, (**c**) 15 and (**d**) 20 min. The diffraction peaks identified from the $CuInSe_2$, ITO and In_2Se_3 are, respectively, marked by ⊕, • and O.

15 and (d): 20 min). The diffraction peaks identified from the ITO are marked with solid circle sign. We found that, after annealing of as-deposited films at 300 °C during 30 min, the ITO substrates retain their initial structure.

As can be seen in figure 2(a–d), all films are polycrystalline in nature and they appear as peaks located at $2\theta \approx 26{\cdot}75$, $44{\cdot}24$, $52{\cdot}68$, $64{\cdot}85$ and $81{\cdot}55°$. These peaks correspond to most intensive peaks given in the JCPDS card no. 40-1487 for $CuInSe_2$ phase in its tetragonal chalcopyrite structure (ICDD No: 40-1487). They are corresponding, respectively, to the (1 1 2), (2 0 4)/(2 2 0), (1 1 6)/(3 1 2), (4 0 0) and (4 2 4) planes. These peaks distinguish the chalcopyrite structure from the sphalerite.

Figure 3 shows XRD scans reflecting only a section of the scan 25–30° for the films related to different deposition times. As can be seen from this figure, in addition to $CuInSe_2$ reflection peaks, the films deposited at 5, 10 and 15 min show a peak situated at $2\theta \approx 29{\cdot}28°$; this peak is attributed to In_2Se_3 binary phase (ICDD No: 72-1469). Guillén *et al* (2000) and Chaure *et al* (2004) indicated that In_2Se_3 phase coexists with $CuInSe_2$ in indium-rich films.

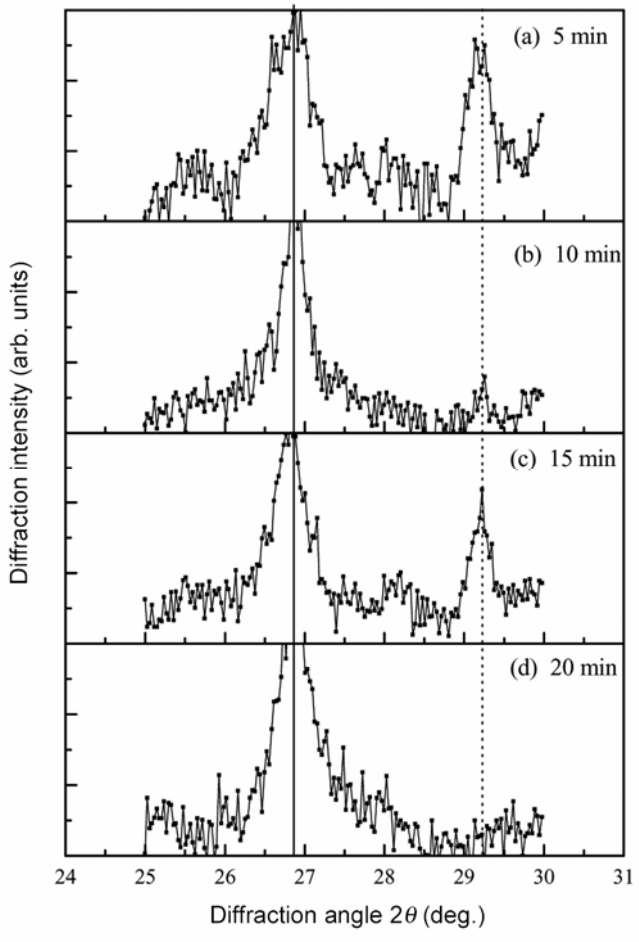

Figure 3. XRD scans reflecting only a section of the scan 25–30° for the films related to different deposition times.

Several workers have reported the appearance of Cu–Se and In–Se binaries phases with $CuInSe_2$. Using photoluminescence and Raman spectroscopy, Niki *et al* (2001) and Volobujeva *et al* (2009) have observed the peaks attributed to binaries CuSe and InSe phases on $CuInSe_2$ surface.

No peaks attributable to Cu–Se binaries phases was detected in our films, because there was a very small amount of these binaries phases that was amorphous or as the $CuInSe_2$ and Cu–Se phases having similar peak positions and, with the available resolution, we were not able to distinguish between these phases.

The variation, as function of deposition time, of peaks intensities of In_2Se_3 and the (1 1 2) peak of chalcopyrite $CuInSe_2$ phases are shown in figure 4. As can be seen, the intensity of (1 1 2) follows the opposite trend of the intensity of In_2Se_3 phase.

The XRD pattern of the film deposited during 20 min (figure 2d) does not appear the peak of In_2Se_3 phase and the intensity of (1 1 2) peak of chalcopyrite $CuInSe_2$ for this film is the highest. This indicates that, among the formation mechanism of $CuInSe_2$, the reaction between the Cu–Se and In_2Se_3 secondary phases according to the following chemical equation (Guillemoles *et al* 1996) is

$$In_2Se_3 + Cu_2Se \rightarrow 2CuInSe_2. \quad (3)$$

Although, to date the reaction mechanism of $CuInSe_2$ formation is still unclear. Mellikov *et al* (2008) indicated that the mechanism of $CuInSe_2$ phase formation in one step electrodeposition goes through a number of consecutive reactions and they confirm the coexistence of $CuInSe_2$ and In_2Se_3 at more negative deposition potentials.

For measurement of the degree of preferential orientation in the films, we defined the variable R_I as the ratio of intensity of (1 1 2) peak to the sum of intensities of all

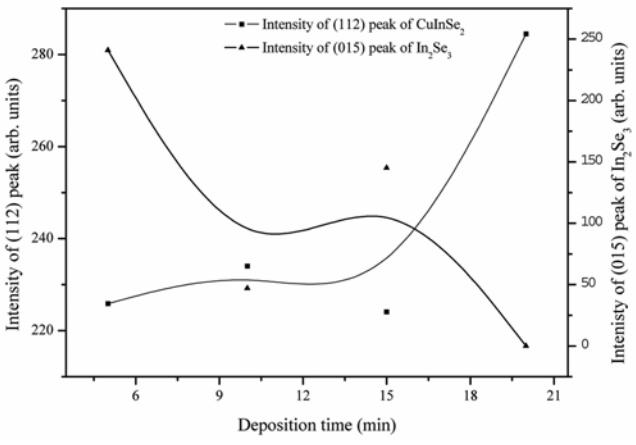

Figure 4. Representation of the intensity of the main $CuInSe_2$ and In_2Se_3 diffraction peak as a function of the deposition time.

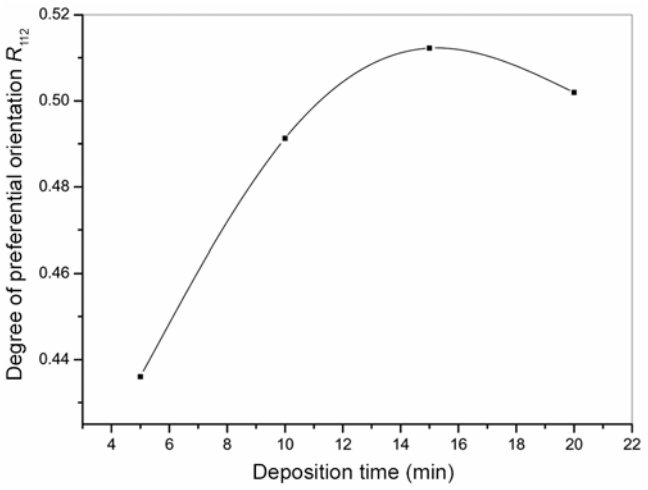

Figure 5. The variations of $R_{(1\,1\,2)}$ of elaborated thin films as a function of deposition time.

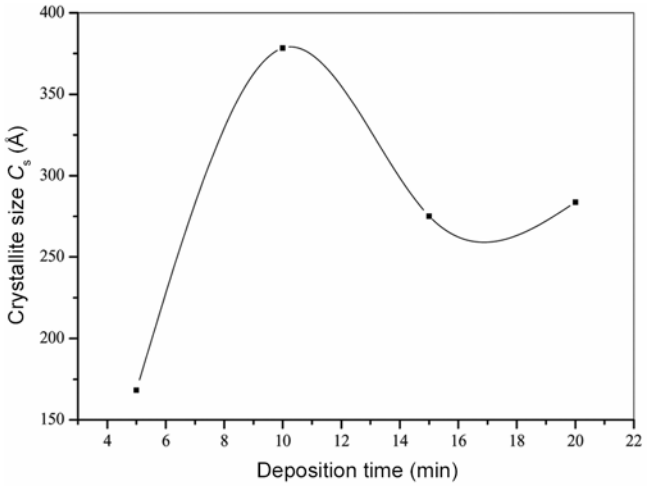

Figure 6. Variation of crystallite size with deposition time.

peaks in the X-ray pattern (Muller *et al* 2006). The variations of $R_{(1\,1\,2)}$ of films as a function of deposition times are depicted in figure 5. As can be seen from this figure, deposition time varies from 5 to 20 min, the $R_{(112)}$ passes from 0·43 to 0·50. These values show the high degree of preferred orientation towards the (1 1 2) direction for all films.

The average crystallite size, C_s, of $CuInSe_2$ films was estimated by using Scherr's formula (Malssel and Glang 1970)

$$C_s = \frac{0{\cdot}9\lambda}{\beta\cos\theta}, \tag{4}$$

where λ is the wavelength of X-ray, β the full width at half maximum in radians of the main peak of the XRD spectrum and θ the Bragg angle. Before calculating the crystallite size, line broadening due to the equipment was substracted from the peak width. Using the crystallite size, C_s, the dislocation density δ and the strain ε in the films are evaluated using the same scheme as described in Dhanam *et al* (2005).

Figure 6 shows the variation of the crystallite size with deposition time. The dislocation density and the strain values are reported in table 1. As can be seen from figure 6, the crystallite size follows the opposite trend of internal strain and the dislocation density. The crystallite size first shows an increasing tendency, reaching a maximum value for 10 min and then shows a decreasing tendency with deposition time from 10 to 20 min.

The change in crystallite size and lattice strain with deposition time could infer that higher the lattice strain, lower will be the crystallite size, suggesting that the decrease implies that lattice strain in films restricts the growth of grains.

The lattice constants a and c for the tetragonal phase structure are calculated from the XRD data using the tetragonal interplanar spacing equation. The cell parameters, a and c, vary, respectively, in 5·74–5·76 Å and 11·52–11·57 Å ranges, similar results have been found by Pal *et al* (1994).

The band gap of the deposited films was determined from the optical absorption spectra. The absorption coefficient, α, in the region of the fundamental band edge, was determined at various photon energies from the transmission spectra using the relation

$$\alpha = \frac{1}{d\ln(1/T)}, \tag{5}$$

where d is the thickness of the film and T the observed transmittance.

The optical band gap, E_g, was deduced from the linear extrapolation of the square of the absorption coefficient vs the photon energy near the band edge using the well-known relationship (Sharma *et al* 1992)

$$\alpha = \frac{C}{h\nu}(h\nu - E_g)^{1/2}. \tag{6}$$

Here C, h and ν represent a constant, Plank's constant and frequency of the incident radiation, respectively. Figure 7(a–d) shows the variation of $(\alpha h\nu)^2$ vs photon energy $(h\nu)$ plot near the band edge. The value of absorption coefficient, α, has been found to be dependent of both radiation and deposition time.

On the contrary, at low absorption levels, the absorption coefficient is described by the Urbach formula (Urbach 1953)

$$\alpha = \alpha_0 e^{h\nu/E_{00}}, \tag{7}$$

where α_0 is a constant dependent on the optical band gap, but independent of photon energy and E_{00}, called Urbach energy, characterizes the disorder in the film

Table 1. The lattice constants (a and c), strain (ε) and dislocation density (δ) vs the deposition time.

Deposition time (min)	a (Å)	c (Å)	Strain, ε ($\times 10^{-4}$ %)	Dislocation density, δ ($\times 10^{15}$ lines m^{-2})
5	5·74	11·55	22	3·53
10	5·76	11·52	10	0·69
15	5·76	11·53	14	1·32
20	5·76	11·57	13	1·24

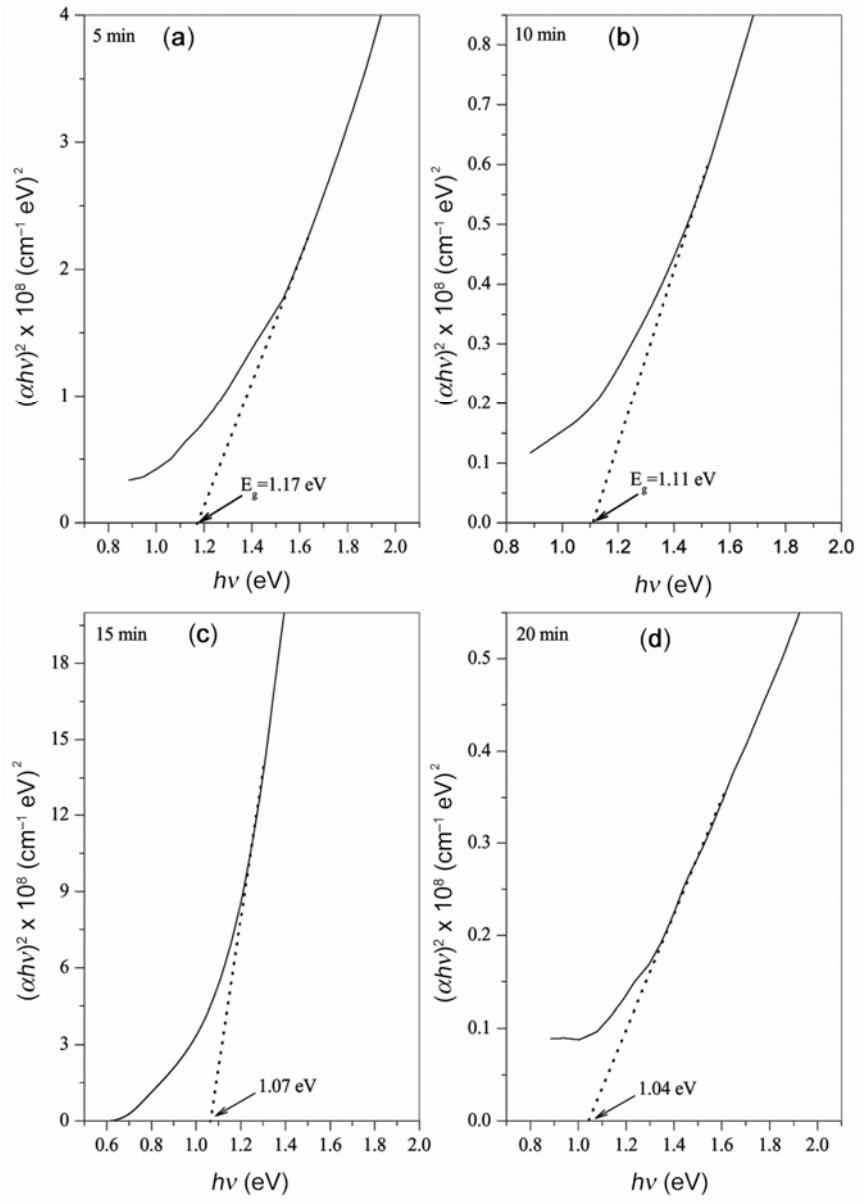

Figure 7. The square of the measured absorption coefficient $(\alpha h\nu)^2$ vs the incident photon energy ($h\nu$) for $CuInSe_2$ film deposited at different times: (**a**) 5, (**b**) 10, (**c**) 15 and (**d**) 20 min.

network. The inverse of the slope from plot of ln(α) vs $h\nu$ gives the value of Urbach energy.

In figure 8, the values of the energy band gap, E_g and Urbach energy, E_{00}, have been reported as a function of deposition time. From the plot, it is seen that the band gap energy decreases linearly with increasing deposition time and it changes inversely with the Urbach energy. This behaviour clearly indicates that the energy band gap

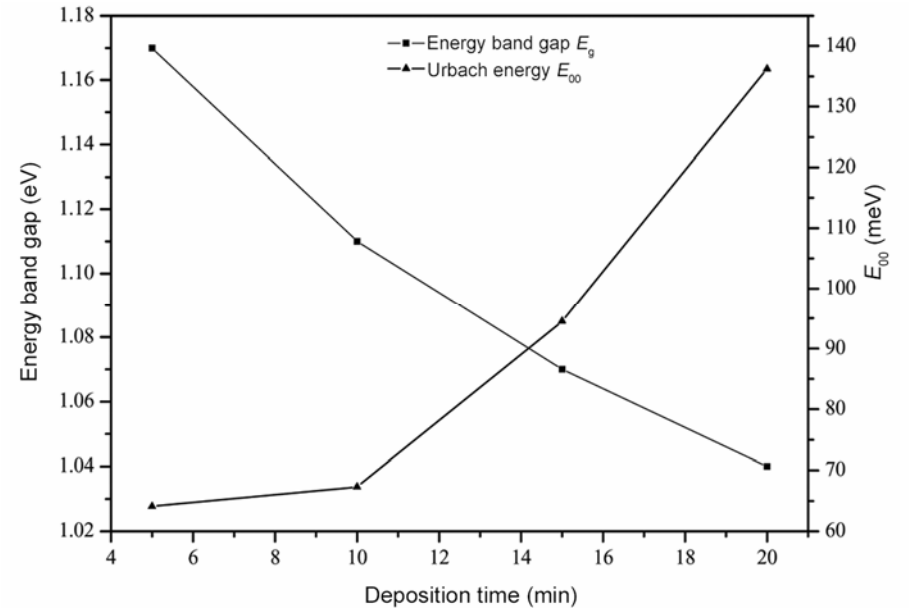

Figure 8. Variation of energy band gap, E_g, and Urbach energy, E_{00}, vs deposition time.

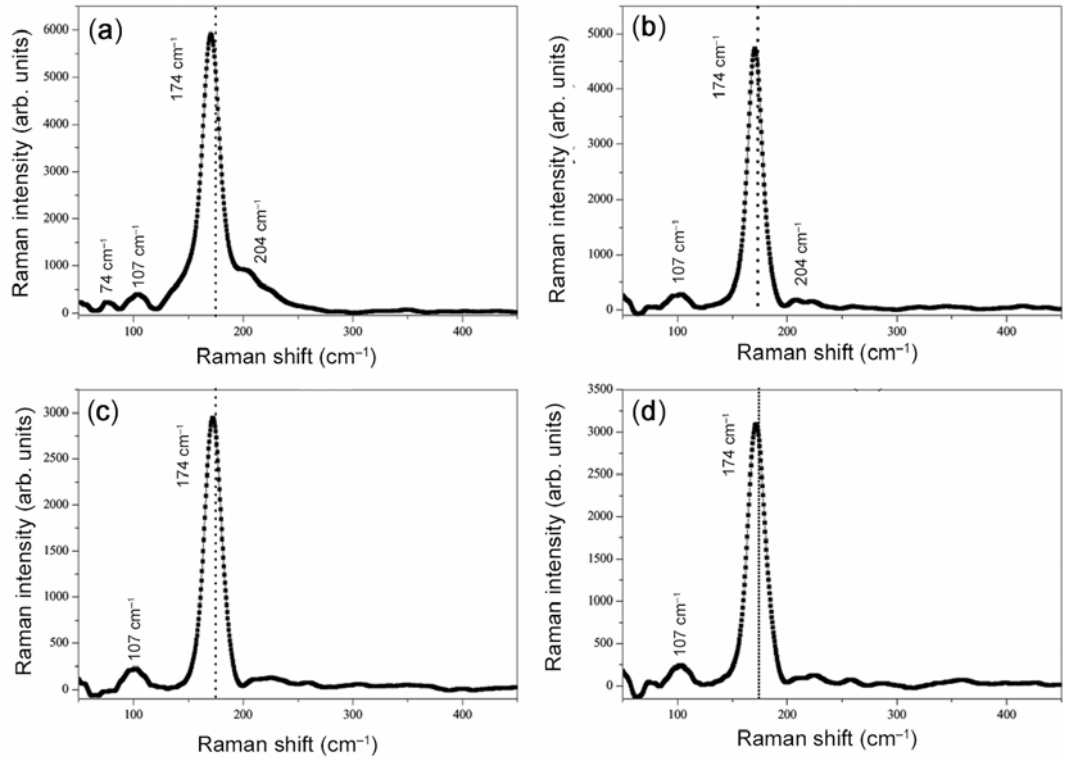

Figure 9. Raman spectra of $CuInSe_2$ thin films deposited at different times: (**a**) 5, (**b**) 10, (**c**) 15 and (**d**) 20 min.

variation in the obtained films is governed by the disorder in film network. The obtained values are in good agreement with the reported values by many workers (Pachori *et al* 1986; Shah *et al* 2009).

The films were also analysed by Raman spectroscopy. The Raman spectra of the films are depicted in figure 9(a–d). In all the Raman spectra, the most intense line is observed at approximately 174 cm^{-1}, which is the

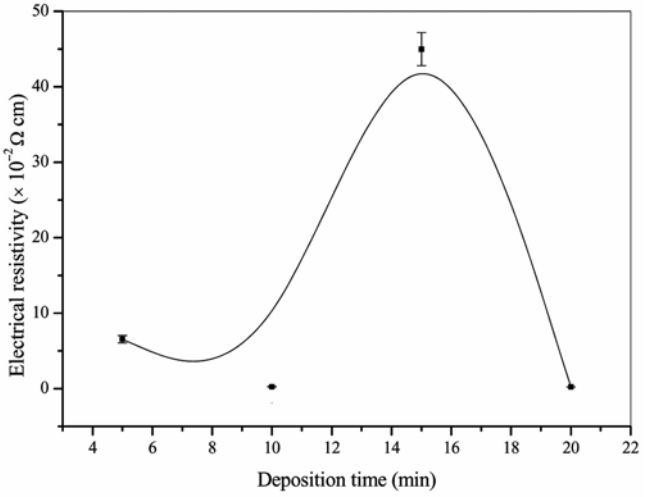

Figure 10. Variation of the room temperature electrical resistivity vs deposition time.

characteristic mode observed in the I–III–IV_2 chalcopyrite compounds. This peak is assigned to the A_1 mode and arises due to the motion of selenium atoms with copper and indium atoms at rest (Zaretskaya *et al* 2003, Chen *et al* 2010; Deepa *et al* 2012). As indicated in XRD results (figure 2(a–d)), the Raman spectra does not show the peaks of Cu–Se secondary phase.

Three peaks situated at 74, 107 and 204 cm^{-1} are observed. These modes are reported to be due to In_2Se_3 binary compounds, although this phase is not observed in the XRD pattern for the film deposited during 20 min (figure 2d) (Julien and Eddrief 1992).

The variation of the room temperature electrical resistivity with deposition time is shown in figure 10. The films exhibited a range of resistivity varying from $2.30 \mp 0.06) \times 10^{-3}$ Ω cm to $(4.49 \mp 0.22) \times 10^{-1}$ Ω cm. As can be seen, the electrical resistivity first shows an increasing tendency, reaching a maximum value for 15 min and then shows a decreasing tendency with deposition time from 15 to 20 min. The slightly resistive films are preferred for device fabrication and the highly conductive films are used as the bottom layer of the absorber near the electrode (Deepa *et al* 2009). The obtained values are in general agreement with other results. Deepa *et al* (2009) have reported that the values vary from 10^{-3} to 10^2 Ω cm for $CuInSe_2$ deposited using sequential evaporation.

From the above results, we have found that the film deposited during 20 min presents single phase, polycrystalline and chalcopyrite $CuInSe_2$ and exhibits better crystallinity and excellent optical properties, it can be used as a good absorber layer in the fabrication of thin film solar cells.

4. Conclusion

Single-phase, polycrystalline and chalcopyrite $CuInSe_2$ thin films with good properties were electrodeposited on ITO-covered glass substrate. All elaborated films present $CuInSe_2$ in its chalcopyrite structure and with preferred orientation along (1 1 2) direction. In the films deposited at 5, 10 and 15 min, In_2Se_3 is present as a secondary phase together with the main $CuInSe_2$ chalcopyrite phase. The In_2Se_3 peak intensity decreases with deposition time and it disappeared for the film deposited at 20 min, indicating that the formation mechanism of $CuInSe_2$ depends on the binary In_2Se_3 phase. The chalcopyrite structure of the films was also confirmed from Raman spectroscopy. We found also that the film deposited during 20 min possesses a band gap of 1·04 eV and can be used as an absorber layer of the solar cell.

References

Chaure N B, Young J, Samantilleke A P and Dharmadasa I M 2004 *Sol. Energy Mat. Sol. Cells* **81** 125

Chen H, Yu S M, Shin D W and Yoo J B 2010 *Nanoscale Res. Lett*. **5** 217

Deepa K G, Jayakrishnan R, Vijayakumar K P, Sudha Kartha C and Ganesan V 2009 *Solar Energy* **83** 964

Deepa K G, Vijayakumar K P and Sudhakartha C 2012 *Mater. Sci. Semiconduct. Proc.* **15** 120

Dhanam M, Manoj P K and Prabhu R R 2005 *J. Cryst. Growth* **280** 425

Fahoume M, Chraibi F, Aggour M and Ennaoui A 1998 *Ann. Chim. Sci. Mater.* **23** 373

Faraday M 1834 *Philos. Trans. R. Soc.* **124** 77

Guillemoles J F, Cowache P, Lusson A, Fezzaa K, Boisivon F, Vedel J and Lincot D 1996 *J. Appl. Phys.* **79** 7293

Guillén C, Martinez M A and Herrero J 2000 *Vacuum* **58** 594

Huang C J, Meen T H, Lai M Y and Chen W R 2004 *Sol. Energy Mater. Sol. Cells* **82** 553

International Center for Diffraction Data, ICDD, PDF2 Database, file number 40-1487 for $CuInSe_2$.

International Center for Diffraction Data, ICDD, PDF2 Database, file number 72-1469 for In_2Se_3.

Julien C and Eddrief M 1992 *Mater. Sci. Eng.* **B13** 247

Kavcar N, Carter M J and Hill R 1992 *Sol. Energy Mat. Sol. Cells* **27** 13

Malssel L I and Glang R 1970 *Handbook of thin film technology* (New York: McGraw Hill Book Company)

Mellikov E *et al* 2008 *Thin Solid Films* **516** 7125

Moharram A H, Hafiz M M and Salem A 2001 *Appl. Surf. Sci.* **172** 61

Moorthy Babu S, Ennaoui A and Ch Lux-Steiner M 2005 *J. Cryst. Growth* **275** 1241

Muller J, Nowoczin J and Schmitt H 2006 *Thin Solid Films* **496** 364

Murali K R 1988 *Thin Solid Films* **167** 19

Niki S, Suzuki R, Ishibashi S, Ohdaira T, Fons P J, Yamada A, Oyanagi H, Wada T, Kimura R and Nakada T 2001 *Thin Solid Films* **387** 129

Pachori R D, Banerjee A and Chopra K L 1986 *Bull. Mater. Sci.* **8** 291

Pal R, Chattopadhyay K K, Chaudhuri S and Pal A K 1994 *Thin Solid Films* **247** 8

Parretta A, Addonizio M L, Agati A, Pellegrino M, Quercia L, Cardellini F, Kessler J and Schock H W 1993 *Jpn. J. Appl. Phys.* **32** 80

Rincon C, Gonzalez J and Sanchez Perez G 1983 *Solid State Commun.* **48** 1001

Shah N M, Ray J R, Patel K J, Kheraj V A, Desai M S, Panchal C J and Rehani B 2009 *Thin Solid Films* **517** 3639

Sharma K C, Sharma R P and Garg C 1992 *J. Phys. D: Appl. Phys.* **24** 1019

Tembhurkar Y D and Hirde J P 1994 *Bull. Mater. Sci.* **17** 465

Urbach F 1953 *Phys. Rev.* **92** 1324

Volobujeva O, Altosaar M, Raudoja J, Mellikov E, Grossberg M, Kaupmees L and Barvinschi P 2009 *Sol. Energy Mat. Sol. Cells* **93** 11

Weast R C (ed.) 1980 *CRC handbook of chemistry and physics* (Boca Raton, FL: CRC)

Wellings J S, Samantilleke A P, Heavens S N, Warren P and Dharmadasa I M 2009 *Sol. Energy Mat. Sol. Cells* **93** 1518

White F R, Clark A H and Graf M C 1979 *J. Appl. Phys.* **50** 544

Zaretskaya E P, Gremenok V F, Riede V, Schmitz W, Bente K, Zalesski V B and Ermakov O V 2003 *J. Phys. Chem. Solids* **64** 1989

Zouaoui A, Lachab M, Hidalgo M L, Chaffa A, Llinares C and Kesri N 1999 *Thin Solid Films* **339** 10